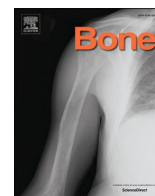| Title	Combination treatment with ibandronate and eldecalcitol prevents osteoporotic bone loss and deterioration of bone quality characterized by nano-arrangement of the collagen/apatite in an ovariectomized aged rat model
Author(s)	Ozasa, Ryosuke; Saito, Mitsuru; Ishimoto, Takuya et al.
Citation	Bone. 157 p.116309
Issue Date	2022-04-01
oaire:version	VoR
URL	https://hdl.handle.net/11094/89751
rights	This article is licensed under a Creative Commons Attribution 4.0 International License.
Note	

Combination treatment with ibandronate and eldecalcitol prevents osteoporotic bone loss and deterioration of bone quality characterized by nano-arrangement of the collagen/apatite in an ovariectomized aged rat model

Ryosuke Ozasa [a], Mitsuru Saito [b], Takuya Ishimoto [a], Aira Matsugaki [a], Yoshihiro Matsumoto [c], Takayoshi Nakano [a,*]

[a] *Division of Materials and Manufacturing Science, Graduate School of Engineering, Osaka University, 2-1 Yamadaoka, Suita, Osaka 565-0871, Japan*
[b] *Department of Orthopaedic Surgery, Jikei University School of Medicine, 3-25-8 Nishi-Shinbashi, Minato-ku, Tokyo 105-8461, Japan*
[c] *Product Research Department, Kamakura Research Laboratories, Chugai Pharmaceutical Co., Ltd., 200 Kajiwara, Kamakura, Kanagawa 247-8530, Japan*

ARTICLE INFO

ABSTRACT

Combination therapy with bisphosphonates and vitamin D_3 analogs has been frequently used for the treatment of osteoporosis. However, its effects on bone anisotropies, such as orientations of collagen and apatite at the nanometer-scale, which is a promising bone quality index, and its trabecular architecture at the micrometer scale, are not well understood despite its important mechanical properties and its role in fracture risk. In the present study, we analyzed the effects of ibandronate (IBN), eldecalcitol (ELD), and their combination on the collagen/apatite orientation and trabecular architectural anisotropy using an estrogen-deficiency-induced osteoporotic rat model. Estrogen deficiency caused by ovariectomy (OVX) excessively increased the degree of collagen/apatite orientation or trabecular architectural anisotropy along the craniocaudal axis in the lumbar vertebra compared to that of the sham-operated group. The craniocaudal axis corresponds to the direction of principal stress in the spine. The excessive material anisotropy in the craniocaudal axis contributed to the enhanced Young's modulus, which may compensate for the reduced mechanical resistance by bone loss to some extent. The solo administration of IBN and ELD prevented the reduction of bone fraction (BV/TV) determined by μ-CT, and combination therapy showed the highest efficacy in BV/TV gain. Furthermore, the solo administration and combination treatment significantly decreased the degree of collagen/apatite orientation to the sham level. Based on the results of bone mass and collagen/apatite orientation, combination treatment is an effective strategy. This is the first report to demonstrate the efficacy of IBN, ELD, and combination treatment with IBN and ELD relative to the bone micro-architectural anisotropy characterized by collagen/apatite orientation.

1. Introduction

Anti-osteoporotic agents have unique effects on bone metabolism, depending on their type. Bisphosphonates are the most commonly used drugs for the treatment of osteoporosis. Furthermore, the combined use of bisphosphonates and vitamin D_3 analogs has been investigated in several preclinical and clinical trials as effective therapeutics for

osteoporosis [1–3]. Ibandronate (IBN), a nitrogen-containing bisphosphonate, was reported to suppress bone resorption and preserve bone mass in intact animals and various animal models of osteoporosis (estrogen deficiency [4], glucocorticoid administration [5], and weightlessness [6]). IBN efficiently targets osteoclasts and inhibits farnesyl diphosphate synthase, an enzyme in the mevalonate pathway, which plays a role in bone lysis [7,8]. Eldecalcitol [1α,25-dihydroxy-2β-

(3-hydroxypropyloxy) vitamin D_3; ELD], an analog of calcitriol [1α,25-dihydroxy vitamin D_3; 1,25(OH)$_2$ D_3], has been reported to inhibit osteoclastogenesis and stimulate bone resorption-independent bone formation (mini-modeling) [9]. The combinatory treatment of IBN and ELD decreases bone resorption without reducing bone formation, compared to monotherapy with either IBN or ELD [1].

Most studies on osteoporotic bone alteration and the effects of therapy with anti-osteoporotic agents have been based on bone mass- or bone mineral density (BMD)-based analyses. However, it has been suggested that analyses from the viewpoint of bone quality are indispensable. Numerous studies on the medicinal efficacy of anti-osteoporotic agents have depicted a disagreement between BMD and bone strength in osteoporosis [10,11], indicating the importance of bone quality [12], i. e., factors other than BMD that contribute to bone strength [13]. Consequently, efforts have recently been made to analyze bone quality in studies on osteoporosis and its treatment. Therefore, changes in bone quality based on alterations in bone materials have begun to be understood. In osteoporotic bones, abnormalities in properties, such as microdamage accumulation [14,15], bone mineralization [16], mineral crystal size [17,18], mineral/collagen ratio [17], collagen cross-linkage [19], and collagen/mineral orientation [20,21] have been reported.

The present study focused on the preferential orientation of the extracellular matrix (ECM), which is predominantly composed of collagen and bone minerals (apatite crystallite), because the degree of collagen/apatite orientation has been shown to correlate with mechanical properties of bone, such as Young's modulus and fracture toughness in several kinds of hard tissues [22–27], including osteoporotic bone [21]. A correlation between collagen/apatite orientation and bone strength is caused by the anisotropic nature of collagen [28] and apatite [29]. Moreover, the crystallographic *c*-axis of apatite lies almost parallel to the collagen fibril axis [30,31] through epitaxial crystallization [32], conforming to collagen/apatite nanocomposites with each strong direction co-aligned within the bone matrix to enhance nanostructural and mechanical anisotropies.

The present study investigated the effects of monotherapy with IBN and ELD, and their combination therapy on osteoporosis induced by estrogen deficiency with a focus on the preferential orientations of collagen and apatite as bone quality. Aged rats were used in this study. Additionally, micro-architectural anisotropy in vertebral trabecular bone was analyzed to comprehensively understand bone structural anisotropy from the nanometer to micrometer scale to determine the fracture risk of osteoporotic bones from a perspective other than bone density.

2. Materials and Methods

In this study, unused bones from animals used in a previous study [1] were analyzed. In this study, we analyzed the preventive effects of IBN, ELD, and their combined administration on ovariectomy (OVX)-induced osteoporosis from novel viewpoints (especially anisotropies in bone trabecular architecture and collagen/apatite nano-arrangement) which were different from the analyses performed in Ref. 1. The findings reported in Ref. 1 are referred to only in Materials and Methods section and Discussion section.

2.1. Animal experiments

A total of forty-five female Wister-Imamichi rats were obtained from the Institute for Animal Reproduction (Ibaraki, Japan). Block randomization was performed using a computer-generated randomization list (SAS Proc Plan; SAS Institute, Inc., Cary, NC, USA), and the 8-month-old rats were randomly divided into five groups. Four groups were ovariectomized to develop a rat model of postmenopausal osteoporosis, and the fifth group was sham-operated. Animals were individually housed under specific pathogen-free conditions in stainless steel cages with a 12 h light/12 h dark cycle throughout the study and allowed to eat (CE-2;

CLEA Japan, Tokyo, Japan) and drink tap water *ad libitum*. To investigate the effects of anti-osteoporotic agents, five groups (n = 9) were prepared as follows: (i) sham, sham-operated; (ii) VEH, OVX treated with vehicle; (iii) IBN, OVX treated with IBN; (iv) ELD, OVX treated with ELD; (v) Combination, OVX treated with IBN plus ELD. From the day after surgery, OVX rats were treated with IBN (subcutaneously, once every 4 weeks, three times in total; 3 μg/kg), ELD (orally, once daily, 15 ng/kg), or their combination for 12 weeks. Isotonic sodium chloride solution and medium-chain triglyceride (MCT; Nisshin OilliO Group, Tokyo, Japan) were used as IBN and ELD vehicles, respectively. 20 mg/kg tetracycline (Sigma-Aldrich, MO, USA) and 10 mg/kg calcein (Dojindo Laboratories, Kumamoto, Japan) were subcutaneously administered, seven and two days prior to the necropsy. Health problems were not observed in any rat. The bodyweight of the VEH group was significantly higher than that of the sham group throughout the experiment. Treatment with IBN, ELD, or their combination does not affect body weight [1]. The third lumbar (L3) and fourth lumbar (L4) vertebral bones and tibiae were extracted from animals immediately after necropsy and fixed with 70% ethanol. In this study, we analyzed the anterior cortex region of the vertebral body because this region mainly bears axial compression or flexion [33]. All animal procedures and protocols were approved by the Institutional Animal Care and Use Committees of Ina Research Inc. and the Chugai Pharmaceutical Co., Ltd.

2.2. Measurement and analysis of trabecular bone architecture

The L4 vertebra was imaged with micro-computed tomography (μ-CT, SMX-100CT; Shimadzu, Kyoto, Japan) to measure the properties of the trabecular bone, including the bone volume fraction (BV/TV), trabecular thickness (Tb.Th), trabecular number (Tb.N), trabecular separation (Tb.Sp), degree of anisotropy (DA), and structural model index (SMI). μ-CT images were obtained at 47 kV and 95 μA, with a resolution of 15 μm voxels. For binarization of the μ-CT images, the threshold value was determined as follows. A histogram curve for the gray value derived from the μ-CT image was fitted to a Gaussian curve. The lowest value between the two peaks derived from bone tissue and for other tissues was used as the threshold for binarization. A series of analyses for the middle part of the L4 vertebra (25% of the full length along the craniocaudal axis) were processed using TRI/3D-BON software (Ratoc System Engineering, Japan).

2.3. Measurement of volumetric bone mineral density (vBMD) and cortical cross-sectional area

vBMD and cortical surface area were measured using a peripheral quantitative computed tomography (pQCT) system (XCT Research SA+; Stratec Medizintechnik GmbH, Birkenfeld, Germany). The mid-transverse sections of the L4 vertebra and tibia were scanned at a resolution of $70 \times 70 \times 260$ μm³. The vBMD values of the anterior cortex of the L4 vertebra were analyzed for the regions with $210 \times t$ μm² (t μm is the cortical thickness along the frontal-horizontal axis, which varies depending on each bone specimen), where the microbeam X-ray diffraction (μ-XRD) analysis was performed. Cortical cross-sectional areas of the L4 vertebra and tibia were determined by counting the voxels with a vBMD of ≥690 mg/cm³. Bone tissue-like tissue, cancellous bone, and cortical bone were defined above a threshold value of 267, 395, and 690 mg/cm³, respectively [34,35].

2.4. Measurement of collagen orientation by the birefringence method

To evaluate the orientation angle of collagen molecules along the craniocaudal axis of the L3 vertebra, the section was observed using a two-dimensional birefringence measurement system (WPA-micro, Photonic Lattice, Miyagi, Japan) attached to an upright microscope (BX60; Olympus, Tokyo, Japan). Birefringence analysis was performed using

WPA-VIEW software (version 2.4.2.9, Photonic Lattice), as previously described [21,36]. The characteristics of the L3 vertebra resembled those of the L4 vertebra [37]; thus, the L3 vertebra was used instead of the L4 vertebra for the observations, and the L4 vertebra was used for other measurements.

2.5. Measurement of preferential orientation of the apatite c-axis by μ-XRD

Two types of measurements were performed using μ-XRD. One analysis determined the degree of preferential orientation of the apatite *c*-axis along the craniocaudal axis within the cortical bone in the L4 vertebra and along the longitudinal bone axis in the tibia using a microbeam μ-XRD system (R-Axis BQ; Rigaku, Tokyo, Japan) with a transmission-type optical system and imaging plate (storage phosphors; Fuji Film, Tokyo, Japan) placed behind the specimen. The detailed conditions for μ-XRD were described in a previous paper [38] with minor modifications based on the bone species. The center section along the bone axis of each bone was the analysis region. The incident beam was focused into a beam spot of 200 μm (for the L4 cortex) or 800 μm (for the tibia cortex) in diameter by a double-pinhole metal collimator. The incident X-ray beam was radiated in the frontal-horizontal axis from the frontal surface for the L4 cortex and in the mediolateral axis from the medial surface at the center of the bone width for the tibia to determine diffraction information along the bone axis. The diffraction data were collected for 600 s (for the L4 cortex) or 60 s (for the tibia) to obtain adequate diffraction intensity. From the obtained diffraction intensity pattern (Debye ring), the two representative diffraction peaks for apatite, (002) and (310), were used for apatite *c*-axis orientation, as previously described [38]. The degree of preferential orientation of the apatite *c*-axis was determined by the intensity ratio of (002)/(310) in the XRD profile.

Another analysis measured the degree of preferential orientation of the apatite *c*-axis along the longitudinal axis of the tibia using μ-XRD (D8 Discover with GADDS, Bruker AXS, WI, Germany) with a reflective-type optical system and a two-dimensional position sensitive proportional counter (PSPC) (Hi-STAR; Bruker AXS, MA, USA). The conditions for μ-XRD were based on a previous study [39]. The incident beam was focused into a beam spot of 50 μm by a metal collimator, radiated in the region labeled with calcein in the mid-transversal section of the tibia to obtain diffraction information from this section. The diffraction data were collected for 1800 s. The two representative diffraction peaks for apatite, (002) and (310), appeared at Bragg angles of 25.9° and 39.8°, respectively, and were detected by swinging the specimen in the appropriate range. The degree of preferential orientation of the apatite *c*-axis was determined by the intensity ratio of (002)/(310) in the XRD profile, as described previously [39].

2.6. Young's modulus measurement by nanoindentation

Mid-transversal sections of the L4 vertebra and tibia were obtained using a microtome (Model 660; South Bay Technology Inc., CA, USA) equipped with a diamond wheel saw (Ted Pella Inc., CA, USA). The cross-sections of the specimens were ground using a series of emery papers with an increasing fineness (#2000 and #4000) followed by mirror polishing using a microcloth (Buehler Ltd., IL, USA) with up to 0.05 μm alumina suspension for the nanoindentation test. The bone specimen surfaces were fully dried with a graded ethanol series (70–100%), fixed on a specimen holder, and maintained at 25 °C for 24 h for thermal stabilization. Dried bone specimens showed increased hardness and Young's modulus [40,41] compared to wet specimens; however, the relative magnitudes of their properties before and after drying were reported to be consistent [40]. The uneven moisture content of each specimen after rehydration was a cause of concern; therefore, fully dried specimens were used in the Young's modulus analysis. The Young's modulus of the specimen was measured along the craniocaudal

axis for the L4 vertebra and the longitudinal axis for the tibia using a nanoindentation system (ENT-1100a; Elionix, Tokyo, Japan) with a Berkovich diamond indenter. Load-depth measurements were performed according to the established condition [42], and Young's modulus was calculated using the method of Oliver and Pharr [43]. Poisson's ratio of bone was assumed to be 0.3, and the region between 95% and 50% of the maximum load was used to calculate the slope of the unloading curve. Five indentations were conducted at the anterior cortex of the L4 vertebra, where the μ-XRD and vBMD measurements and the calcein-labeled region in the tibia were performed, and the results were averaged.

2.7. Evaluation of osteocyte viability

L3 vertebral bones were stained using the method described by Villanueva [44]. After dehydration with ethanol and acetone, the specimens were embedded in methyl methacrylate (Wako Pure Chemical Industries, Osaka, Japan). Midsagittal sections of L3 (5 μm thick) were obtained using a microtome (Reichert-Jung 2050 Supercut; Leica, Heidelberg, Germany). Bright-light field images of midsagittal sections of the L3 vertebral bone (5 μm thick) were obtained using a fluorescent microscope (Biozero; Keyence, Osaka, Japan) and processed using Adobe Photoshop 10.0 software (Adobe Systems, San Jose, CA). Based on osteocyte morphology observed under Villanueva staining, normal and atypical osteocytes were determined as previously described [45], and the number of cells with each condition was counted.

2.8. Statistical analysis

Nine animals were used in each group to acquire the data, which were averaged and are presented as the mean ± standard error (S.E.). Normality tests were conducted before data comparisons among the five groups. When a normal distribution was confirmed, comparisons among the five means were performed using one-way analysis of variance (ANOVA). Post-hoc Tukey HSD comparisons or Games–Howell comparisons were conducted according to the test for homoscedasticity. When normal distribution was not assumed, the Kruskal–Wallis test, followed by the Dunn–Bonferroni test was performed for multiple comparisons. Single and multiple regression analyses were performed to determine the factors contributing to Young's modulus. To detect multicollinearity prior to multiple regression analysis, *tolerance* and *variance inflation factors* (*VIF*) were calculated, and *tolerance* values < 0.10 and *VIF* values greater than 10 were considered to indicate a multicollinearity problem according to a previous study [46]. A *p*-value of < 0.05 was considered statistically significant. SPSS software version 25 (SPSS Japan Inc., Japan) for Microsoft Windows was used for the statistical analyses.

3. Results

3.1. Trabecular volume and architecture of L4 vertebra

In this study, μ-CT analyses were performed to evaluate the effect of anti-osteoporotic agents on the trabecular architecture of the L4 vertebral bone (Fig. 1). The VEH group showed decreased BV/TV, Tb.Th, and Tb.N, and increased Tb.Sp compared with the sham group (Fig. 1B). In contrast, all treatment groups suppressed bone loss caused by estrogen deficiency. IBN treatment maintained the sham levels in all parameters of trabecular bone, and the ELD treatment increased Tb.Th compared with that in IBN treatment. The combined treatment of IBN and ELD increased BV/TV compared to the other groups because of the positive effect on Tb.Th and Tb.N. These results indicated that dual administration of IBN and ELD had the greatest effect on bone mass gain under estrogen-deficient conditions. The VEH group exhibited greater values for DA and SMI, indicating that trabecular anisotropy was apparent, and its shape tended to be rod-like under estrogen deficiency. All treatment

A
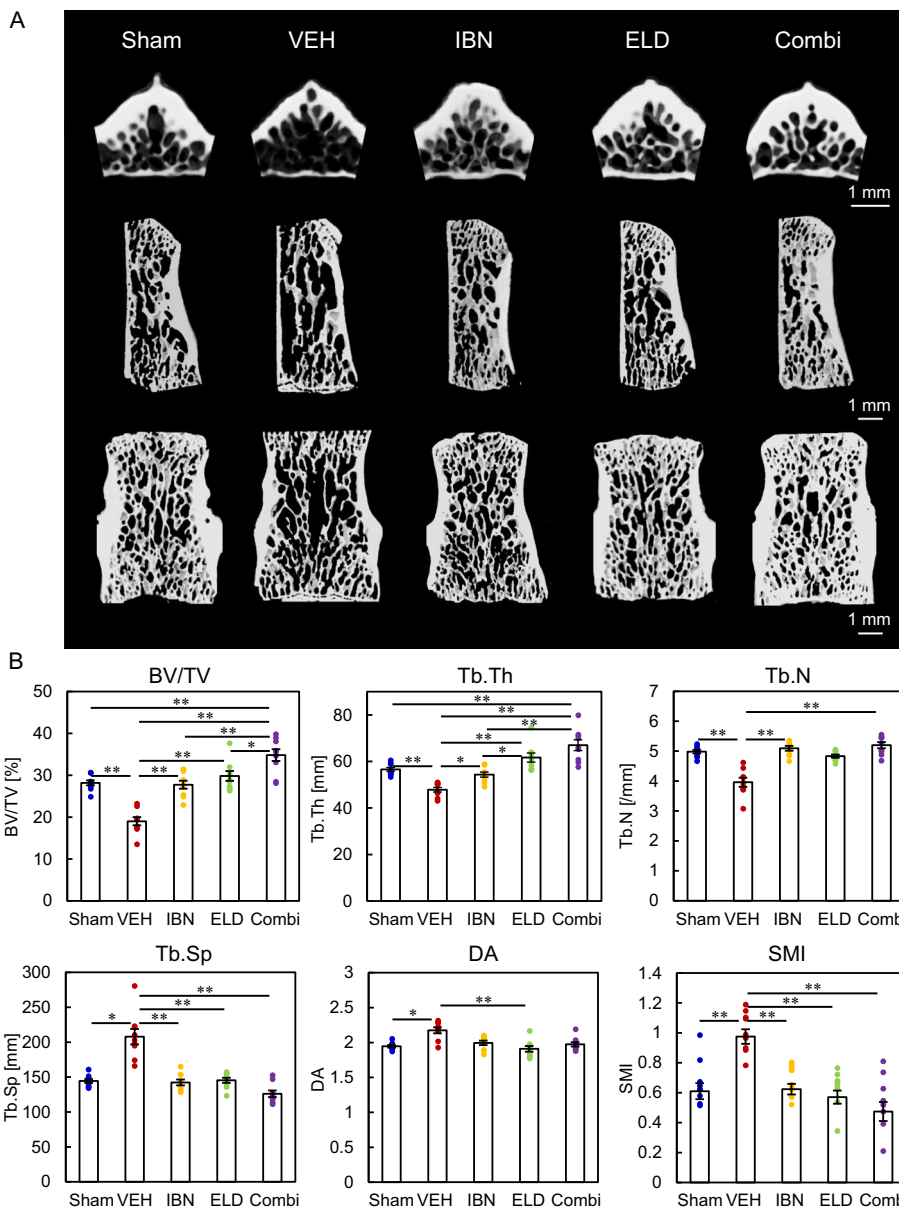
Fig. 1. Three-dimensional trabecular architecture of the L4 vertebrae. (A) Representative micro-computed tomography (μ-CT) images of the L4 vertebral body in each group of mid-transversal (upper row), midsagittal (middle row), and coronal (lower row) sections. (B) Trabecular bone parameters via μ-CT of the middle part of vertebrae along the bone length. BV/TV: bone volume fraction, Tb.Th: trabecular thickness, Tb.N: trabecular number, Tb.Sp: trabecular separation, DA: degree of anisotropy, SMI: structure model index. *: $p < 0.05$, **: $p < 0.01$. Data are represented as the mean ± S.E. (n = 9).

B

groups maintained them at the sham level. These results indicate that treatment with IBN, ELD, or their combination resulted in maintenance of normal trabecular architecture.

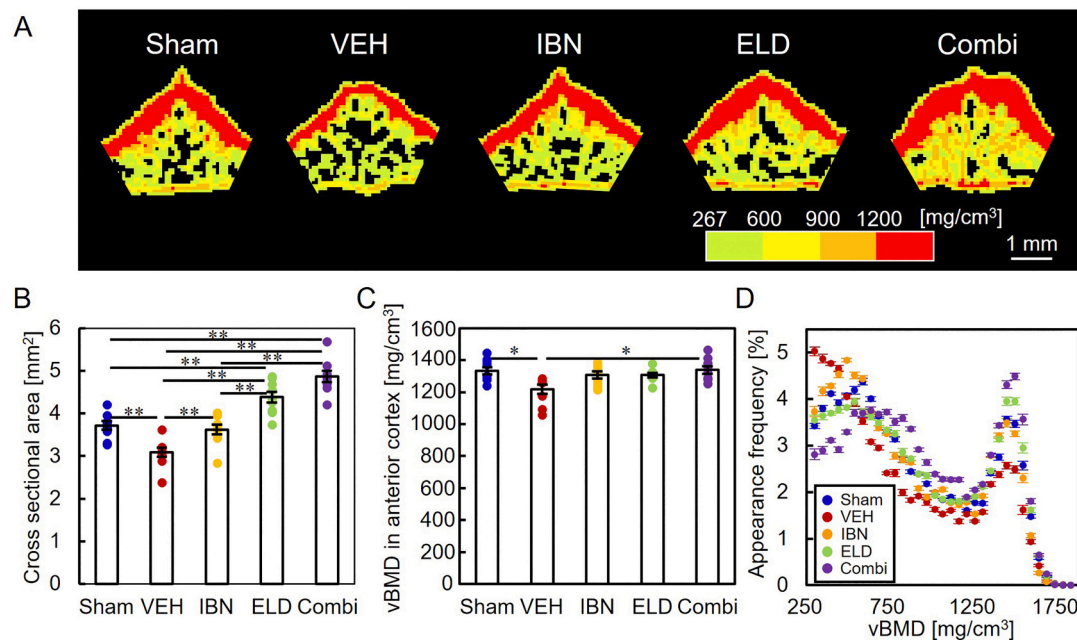### 3.2. Cross-sectional area and vBMD of L4 vertebral cortex

Fig. 2 shows the cross-sectional area and vBMD of the L4 vertebral cortex in the experimental groups. The VEH group had a lower cortical cross-sectional area for the vertebral body (Fig. 2A, B) and exhibited a lower vBMD in the anterior cortex (Fig. 2C) than the sham bone. The treatments offset the bone loss in the VEH group, and the cortex area was increased by ELD treatment. Furthermore, the combined treatment with IBN and ELD had a synergic effect on cortical bone gain (Fig. 2B) and increased vBMD compared to the VEH group (Fig. 2C). The percentage of the cortex area (vBMD ≥ 690 mg/cm^3) to the vertebral bone area prominently increased by the combination treatment (Fig. 2D).

3.3. Preferential collagen/apatite orientation along the craniocaudal axis of the L4 vertebral cortex
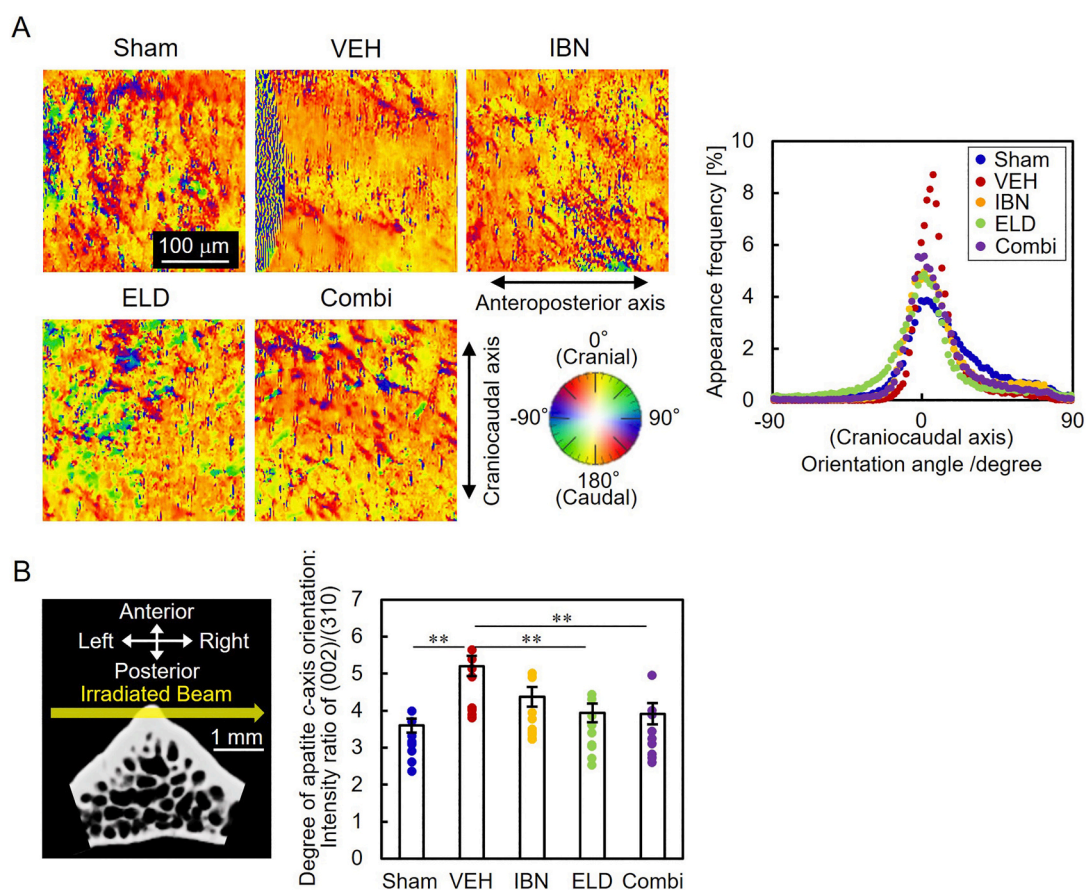
Fig. 3 shows the preferential orientation of collagen/apatite in the vertebral cortex analyzed along the craniocaudal axis. The color mapping images indicate the collagen orientation angle against the craniocaudal axis (Fig. 3A). The orientation angle of collagen peaked at 0° (parallel to the craniocaudal axis) in all experimental groups; however, the degree differed depending on the experimental group. In the VEH group, the degree of collagen and apatite *c*-axis orientation was elevated beyond the sham level (Fig. 3A, B), which agrees with a previous study [21]. Treatment with ELD and its combination with IBN maintained intact degrees of collagen/apatite orientation (Fig. 3A, B). The administration of 3 mg/kg of IBN suppressed the excessive anisotropy of bone material property in the cortex caused by estrogen deficiency, but the difference was not statistically significant (Fig. 3B).

3.4. Young's modulus of the L4 vertebral cortex and its contributors
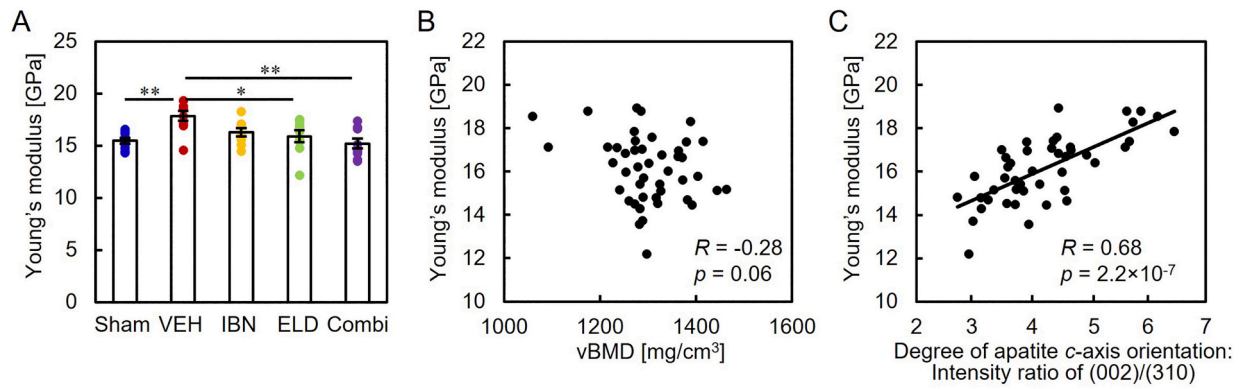
Fig. 4A shows Young's modulus as a material strength of the L4

Fig. 2. Bone densitometric analysis for the cortical bone of the L4 vertebrae. (A) Typical peripheral quantitative computed tomography (pQCT) images of the L4 vertebral body in each group. (B) Variation in cross sectional area of the cortex and (C) volumetric bone mineral density (vBMD) measured within the anterior cortex. (D) Distribution of vBMD of L4 vertebral body. *: $p < 0.05$, **: $p < 0.01$. Data are represented as the mean $\pm$ S.E. (n = 9).

Fig. 3. Preferential orientations of collagen and apatite crystallites along craniocaudal axis analyzed within anterior cortex of vertebral body. (A) Birefringence measurement for analyzing collagen molecular orientation. Color in color mapping images and distribution indicate the collagen orientation angle against the craniocaudal axis. (B) Apatite c-axis orientation analyzed by X-ray diffraction. Incident X-ray beam was radiated into anterior cortex from left to right of L4 vertebrae. **: $p < 0.01$. Data are represented as mean $\pm$ S.E. (n = 9).

Fig. 4. Material strength of the bone matrix in the L4 vertebral body. (A) Young's modulus as bone material strength along the craniocaudal axis analyzed within the anterior cortex of the L4 vertebral body. Relationships for (B) volumetric bone mineral density (vBMD) and (C) degree of apatite *c*-axis against Young's modulus. *: *p* < 0.05, **: *p* < 0.01. Data are represented as the mean ± S.E. (n = 9).

vertebral cortex analyzed along the craniocaudal axis. The modulus in the VEH group was higher than that in the sham bone, which could be due to the degree of apatite *c*-axis orientation. All the treatment groups maintained their modulus at the intact sham level. In this study, no multicollinearity was found between vBMD and the degree of apatite *c*-axis orientation (*Tolerance* = 0.90 ≥ 0.1, *VIF* = 1.1 < 10); therefore, these parameters were used as explanatory variables in the regression analyses of Young's modulus. From the single regression analysis, apatite *c*-axis orientation was significantly and positively correlated with Young's modulus (Fig. 4C), whereas vBMD was not (Fig. 4B). Multiple regression analysis revealed that the preferential orientation of apatite dominantly contributed to Young's modulus ($\beta = 0.66, p = 1.5 \times 10^{-6}$).

3.5. Bone characteristics of cortical bone in the tibia

Fig. 5 shows the characteristics of the cortical bone in the tibial midshaft, including bone surface area, vBMD, the degree of apatite *c*-axis orientation, and Young's modulus analyzed along the longitudinal bone axis of the tibia. The treatment with IBN plus ELD was the most effective in increasing the cortical cross-sectional area, but the increment in the VEH group was less in the tibia (Fig. 5A; + 9.8%) than that in the vertebra (Fig. 2B; + 57.9%). vBMD (Fig. 5B) and apatite *c*-axis orientation (Fig. 5C) were not affected in the tibia. It appeared that the bone characteristics of the tibia were less affected by estrogen deficiency or administration of anti-osteoporotic agents than the vertebral body. In all the experimental groups, calcein-labeled bone formed under each treatment condition was observed at the cortical edge of the medial region (Fig. 5D). Thus, we additionally examined the apatite *c*-axis orientation and Young's modulus at the site (within 50 μm from the endosteum) of the tibia (Fig. 5E). The analysis for vBMD could not be performed because the area of interest was smaller than the $70 \times 70 \ \mu m^2$ resolution of the pQCT analysis in this study. The material anisotropy of calcein-labeled bone along the bone longitudinal axis, which could be assessed by the degree of apatite *c*-axis orientation and Young's modulus, was increased significantly in the VEH group compared to the sham group, and the drug treatment groups maintained moduli at the sham level (Fig. 5F–H).

4. Discussion

The effect of the administration of both IBN and ELD on the prevention of osteoporotic bone changes, especially bone quality, has not been previously investigated. Because 8-month-old rats were used at the start of the study, skeletal growth-dependent effects, which may have influenced the results, were neglected in this study. Our study demonstrated that the combined administration of IBN and ELD effectively

prevented bone quality degradation, characterized by the preferential orientation of collagen/apatite in the lumbar vertebra and the tibia, and deterioration of trabecular architecture and bone loss, using aged OVX rats. The advantage of combination therapy over monotherapy was particularly evident in BV/TV, representing the potential of combination therapy in preventing osteoporotic changes, although solo administration of IBN and ELD also showed significant suppression of these changes. The changes caused by OVX and treatment with anti-osteoporotic agents are summarized in Fig. 6. The BV/TV vs. DA and BMD vs. ECM orientation as bone material parameters were plotted to better understand the changes.

OVX significantly reduced BV/TV of the vertebral trabecular bone, and singular administration of IBN or ELD increased it to a level comparable to that of the sham group. The combined administration of IBN and ELD increased BV/TV beyond the intact level. This decrease/increase in BV/TV can be explained by the decrease/increase in Tb.Th and Tb.N. Similar changes were observed in the cortical bone area, representing the benefit of combined administration of IBN and ELD for bone mass under the condition of estrogen deficiency.

Bisphosphonates have been reported to induce apoptosis of mature osteoclasts after their incorporation into the cell [47] and stimulate the secretion of bone resorption inhibitors from osteoblasts [48]. In particular, IBN has a stronger effect on the inhibition of bone resorption than alendronate, pamidronate, and clodronate [7,49]. However, ELD inhibits osteoclastogenesis by suppressing cell differentiation [50,51], cell migration [52], and RANKL (receptor activator of NF-κB ligand) expression in bone tissue [53]. Thus, the anti-resorptive mode is temporally different between IBN and ELD, by which the synergic suppression of bone resorption by IBN and ELD might be realized, as reported previously [1]. Additionally, ELD suppresses bone resorption by osteoclasts and stimulates mini-modeling, which is bone resorption-independent bone formation [1,9]. Consequently, the combined administration of IBN and ELD resulted in a synergistic improvement in BV/TV.

Regarding trabecular bone structure, DA, and SMI were significantly increased by OVX, and were suppressed by the administration of IBN, ELD, and their combination. An increase in DA caused by OVX represents an enhancement in the anisotropy of the trabecular architecture with respect to the craniocaudal axis, which corresponds to the principal stress direction [54]. As previously documented in osteoporosis, this change in DA and SMI might result from the disappearance of secondary trabeculae that run perpendicular to the craniocaudal axis and thereby increase the proportion of primary trabeculae, [55,56]. This change in DA and SMI is considered part of the bone response to maintain mechanical stiffness against craniocaudally loaded stress, even when bone mass is reduced because of osteoporosis. Note that the use of an ellipsoid factor [57] may more directly capture the changes in trabecular bone
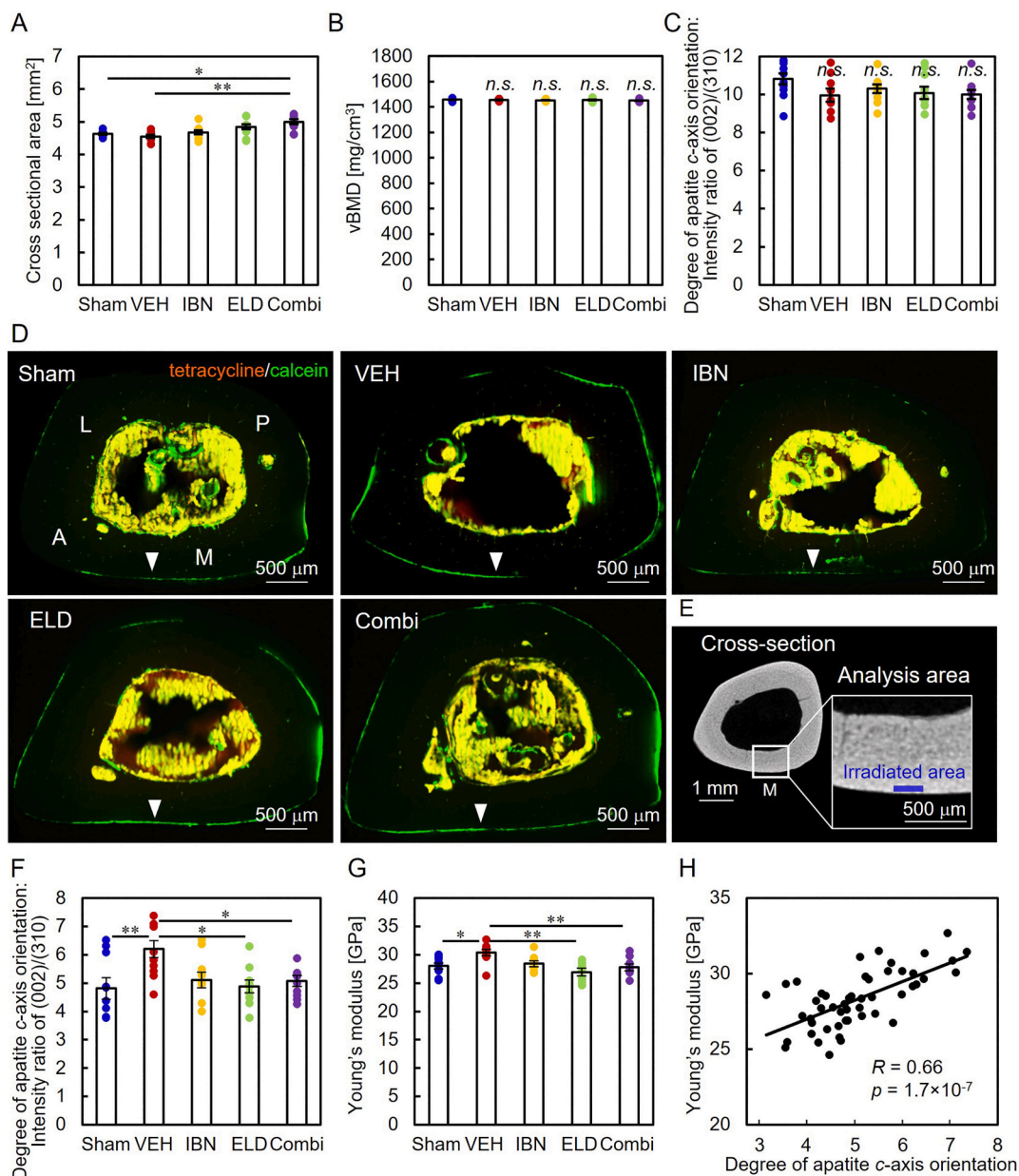
Fig. 5. Bone material properties in the cortex of tibia. (A) Cortical cross-sectional area, (B) volumetric bone mineral density (vBMD), and (C) degree of apatite *c*-axis orientation. (D) Cross-sectional fluorescent images of the tibia, where the fluorescent label is seen in the medial region of the bone (white arrowheads) in all groups. (E) The part filled with blue in the micro-computed tomography (μ-CT) image, which corresponds to the calcein labeled-region in (D), was analyzed. (F) Preferential orientation of apatite *c*-axis and (G) Young's modulus. (H) Correlation between Young's modulus and the degree of apatite *c*-axis orientation. A: anterior; P: posterior; L: lateral; M: medial. *: $p < 0.05$, **: $p < 0.01$, *n.s.*: non significant. Data are represented as the mean ± S.E. (n = 9).

architecture associated with osteoporosis progress and treatment.

Interestingly, in the cortical bone of the vertebral body, as with cancellous bone, bone anisotropy along the craniocaudal axis became prominent simultaneously with the decrease in bone mass (thinning of the cortex). Namely, the preferential collagen/apatite orientation along the craniocaudal axis was significantly enhanced because of OVX. Because the enhancement of preferential collagen/apatite orientation represents an increased Young's modulus in the orientation direction, this material change could also be a bone response to resist bone loss. Such changes in bone anisotropy could be a type of functional adaptation to the increase in stress occurring due to bone loss, for which the integrity of osteocytes, known as mechanosensory cells, is suggested to be important [58]. In the present study, osteocytes in all groups were normal (Fig. 7).

The previous studies also demonstrated the excess enhancement of

the ECM orientation under OVX conditions occurs regardless of animal species (primate or rodent) or age as observed in 6-week-old young rats (OVX for 6 months) [21], 11-month-old mature rats (OVX for 6 months) [20], and 9–17-year-old monkeys (OVX for 17 months) [59]. More importantly, in humans, it has been reported that an enhancement in the apatite orientation under osteoporosis occurs in the vertebral trabeculae [60].

Enhanced mechanical properties only in a certain direction, due to formation of excessive structural and material anisotropies, result in increased fracture risk when subjected to stress in uncommon directions [55], which is generated by, for example, a fall. Hence, it is not a mechanical advantage for bone in which anisotropy increases beyond the optimum extent. Furthermore, the heterogeneity of the material microstructure hinders the propagation of damage and leads to bone toughening [61]; however, OVX produces a more uniform directionality
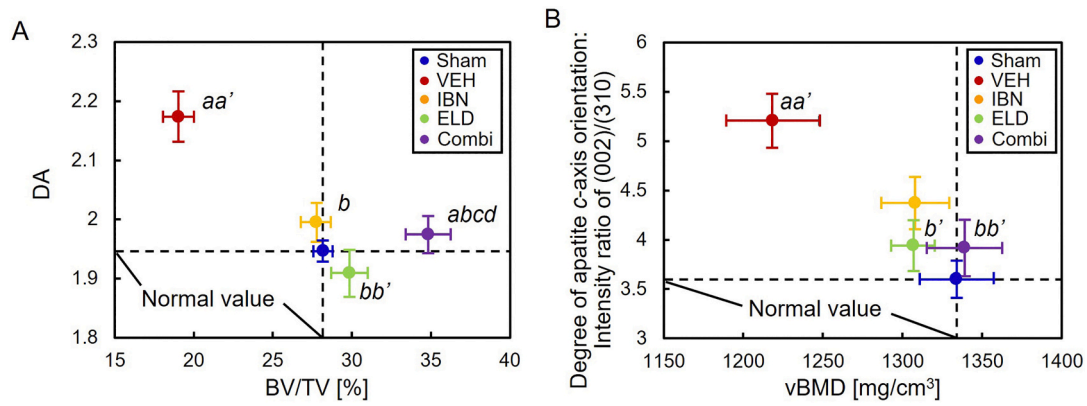
Fig. 6. Effects of drug administration on bone mass (mineral volume and density), trabecular anisotropy and the degree of apatite *c*-axis orientation in the cortical bone of the L4 vertebral bone. (A) BV/TV vs. DA in the trabecular bone. (B) vBMD vs. degree of apatite *c*-axis orientation in the cortical bone. Dashed lines in each graph indicate moderate value based on sham data. The values of DA and BV/TV in Fig. 2, the cortical bone area and vBMD in Fig. 3, and the degree of apatite *c*-axis orientation in Fig. 4 are plotted in this figure. BV/TV: bone volume fraction, DA: degree of anisotropy, vBMD: volumetric bone mineral density; a: $p < 0.05$ vs. Sham; b: $p < 0.05$ vs. VEH; c: $p < 0.05$ vs. IBN; b: $p < 0.05$ vs. ELD in comparison of the value represented in the horizontal axis and a': $p < 0.05$ vs. Sham; b': $p < 0.05$ vs. VEH in the comparison of the value represented by the vertical axis. Data are represented as mean ± S.E. (n = 9).
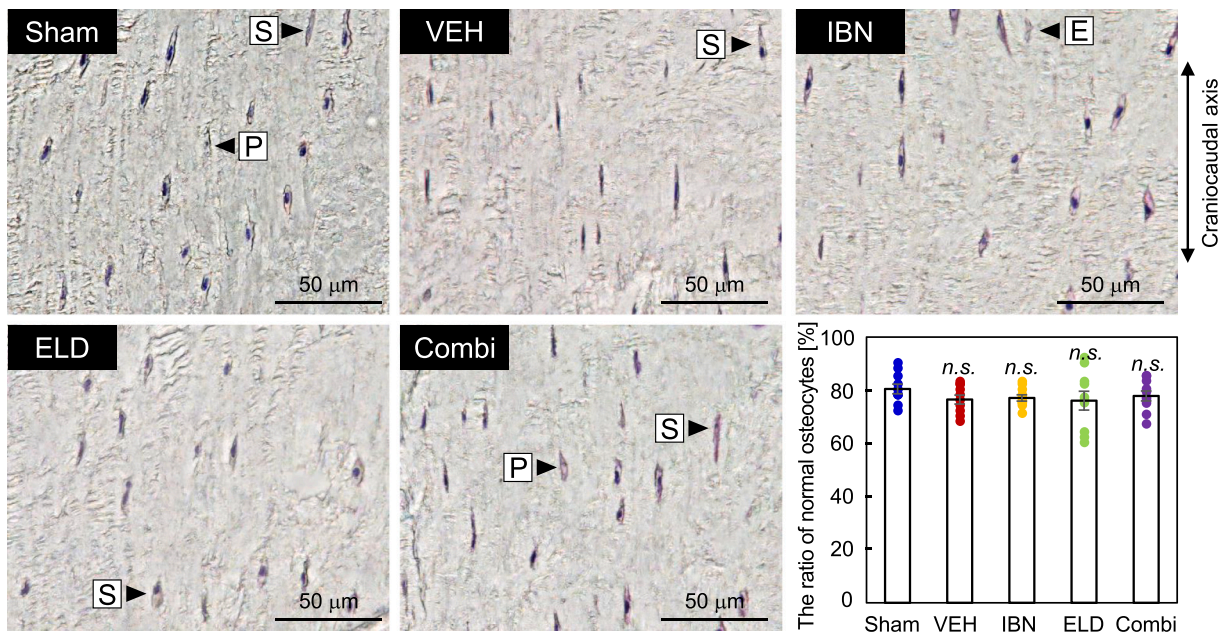
Fig. 7. Effect of drug administration on osteocyte condition. The ratio of normal osteocytes (other than atypical osteocytes) to total osteocytes were counted according to osteocyte morphology observed by bright-field images [42]. Arrowheads in the images indicate atypical osteocytes (S: lacuna with shrunken osteocyte, E: empty lacunae, P: osteocyte with pyknotic nuclei). *n.s.*: non-significant. Data are represented as mean ± S.E. (n = 9).

in the collagen orientation, as is shown in Fig. 3A.

Drug therapies help prevent the formation of abnormal anisotropy. Although IBN alone was insufficient in some measured indices, bone anisotropy was completely normal when combined with ELD. Maintaining anisotropy at a normal level is critical to the mechanical integrity of bone, and combination therapy of IBN and ELD effectively enables this, as summarized in Fig. 8.

It has been reported that the combination therapy of bisphosphonate and the vitamin D_3 analog has an advantageous effect on bone mass and mechanical strength compared to the single administration of each [1,9]. In addition to the preventive effect of osteoporosis shown in this study, the effectiveness of combined administration for recovery of bone mass and strength has also been shown to have a therapeutic effect [20,62]. Moreover, it has been shown that combined administration of risedronate and alfacalcidol more effectively prevents excessive anisotropy of the ECM arrangement than monotherapy with either drug [20].

In the cortex of the long bone midshaft, local areas where the effects of OVX and anti-osteoporotic agents appear (the area where the calcein label was seen), showed an enhanced degree of ECM orientation and Young's modulus along the principally loaded bone longitudinal axis (Fig. 5F), which is similar to the change seen in vertebral bone. However, there was not a significant difference in ECM orientation when taken from the entire cross-section of the tibia (Fig. 5C). The biological response to osteoporosis and its medication is the same in the vertebrae and diaphysis of the long bones despite the difference in bone turnover rate [34].

First, there are multiple characteristics of bone quality (e.g., microdamage, collagen cross-linking), so the present study did not investigate other potential mechanisms of action by which the selected drugs promote fracture resistance of bone. Second, this study did not investigate any osteoporosis models other than estrogen deficiency derived from OVX. In particular, ELD is a vitamin D_3 analog; therefore, different
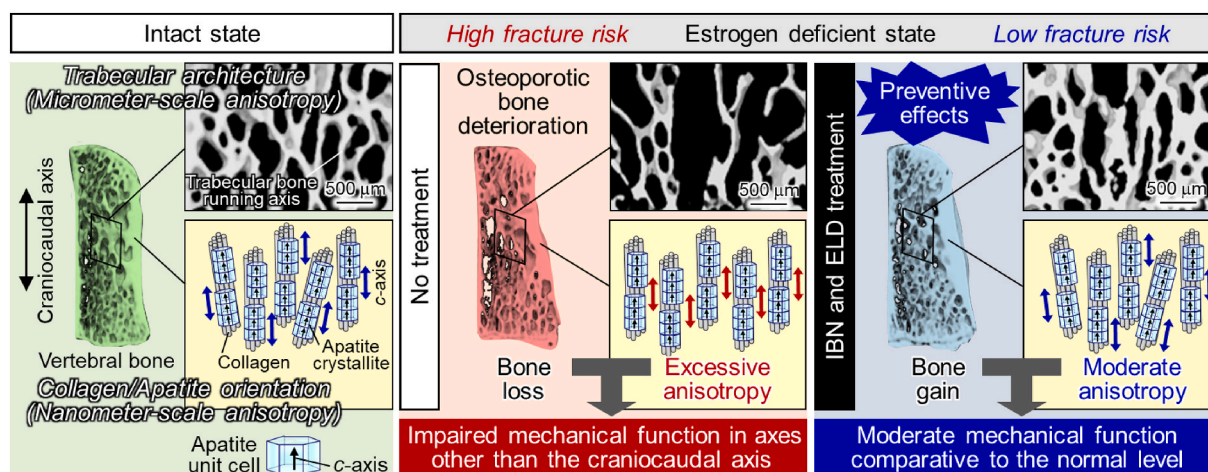
Fig. 8. A schematic illustration of the preventive effects of combinatory treatment of ibandronate (IBN) and eldecalcitol (ELD) on abnormalities of bone mass and bone quality featured by the trabecular architecture and collagen/apatite orientation along the craniocaudal axis because of estrogen deficiency-induced osteoporosis.

effects may occur in osteoporosis where vitamin D$_3$ deficiency is involved. Third, fully dried bone specimens were used to determine Young's modulus, which might result in non-physiological mechanical properties. A nanoindentation test in a humid environment [40,41] was better. Since ELD treatment is effective in patients with vitamin D deficiency, the maintained level of vitamin D in the ovariectomized model [63] may obscure the effects of ELD on bone microarchitecture. The validity of the combination of ELD and IBN needs to be clarified through the use of an ovariectomized rat model with vitamin D deficiency [64] in future research.

The collagen/apatite orientation (anisotropy of collagen/apatite nano-arrangement) varies depending on the bone type and anatomical site to accommodate the stress distribution [22]; that is, the collagen/apatite orientation is formed to exhibit a mechanical functional advantage to local stress directionality, which is why considering collagen/apatite orientation in addition to BMD is essential in discussing the mechanical bone function. To date, anti-osteoporotic agents have been developed based on bone mass or BMD, but the orientation of bone collagen/apatite, as shown in this study, could be an important criterion. However, the currently selected drugs maintained normal collagen/apatite orientation, and combined administration further enhanced the effect; thus, the present osteoporosis therapy was effective. We believe that it is necessary to deepen our understanding of bone quality in other diseases and their therapeutics for developing better medical strategies in the near future.

Disclosure statement

TN and MS have received research support from Chugai Pharmaceutical Co., Ltd. YM is an employee of Chugai Pharmaceutical Co., Ltd. RO, TI and AM have no conflicts of interest to declare.

CRediT authorship contribution statement

Ryosuke Ozasa: Data curation, Formal analysis, Investigation, Methodology, Visualization, Writing – original draft, Writing – review & editing. **Mitsuru Saito:** Formal analysis, Investigation, Methodology, Writing – review & editing. **Takuya Ishimoto:** Data curation, Formal analysis, Investigation, Validation, Visualization, Writing – original draft, Writing – review & editing. **Aira Matsugaki:** Investigation, Resources, Validation, Visualization, Writing – review & editing. **Yoshihiro Matsumoto:** Resources, Validation, Writing – review & editing. **Takayoshi Nakano:** Conceptualization, Methodology, Project administration, Resources, Supervision, Validation, Writing – original draft,

Writing – review & editing.

References

[1] S. Sakai, S. Takeda, M. Sugimoto, M. Shimizu, Y. Shimonaka, K. Yogo, J. Hashimoto, F. Bauss, K. Endo, Treatment with the combination of ibandronate plus eldecalcitol has a synergistic effect on inhibition of bone resorption without suppressing bone formation in ovariectomized rats, Bone 81 (2015) 449–458, https://doi.org/10.1016/j.bone.2015.08.004.

[2] J. Takada, H. Wada, K. Iba, K. Sasaki, T. Dohke, K. Kanaya, T. Yoshizaki, T. Yamashita, Combined use of ibandronate and eldecalcitol in postmenopausal Japanese women with osteoporosis, J. Orthop. Surg. 24 (3) (2016) 362–366, https://doi.org/10.1177/1602400318.

[3] Y. Ono, N. Miyakoshi, Y. Kasukawa, Y. Imai, H. Nagasawa, H. Tsuchie, M. Akagawa, I. Nagahata, Y. Yuasa, C. Sato, M. Kawatani, Y. Shimada, Micro-CT imaging analysis for the effects of ibandronate and eldecalcitol on secondary osteoporosis and arthritis in adjuvant-induced arthritis rats, Biomed. Res. 40 (5) (2019) 197–205, https://doi.org/10.2220/biomedres.40.197.

[4] F. Bauss, S. Lalla, R. Endele, L.A. Hothorn, Effects of treatment with ibandronate on bone mass, architecture, biomechanical properties, and bone concentration of ibandronate in ovariectomized aged rats, J. Rheumatol. 29 (2002) 2200–2208.

[5] K.-J. Zhang, J. Zhang, Z.-K. Kang, X.-M. Xue, J.-F. Kang, Y.-W. Li, H.-N. Dong, D.-G. Liu, Ibandronate for prevention and treatment of glucocorticoid-induced osteoporosis in rabbits, Rheumatol. Int. 32 (11) (2012) 3405–3411, https://doi.org/10.1007/s00296-011-2074-9.

[6] L. Schultheis, C.B. Ruff, S. Rastogi, S. Bloomfield, H.A. Hogan, N. Fedarko, M. Thierry-Palmer, J. Ruiz, F. Bauss, J.R. Shapiro, Disuse bone loss in hindquarter suspended rats: partial weightbearing, exercise and ibandronate treatment as countermeasures, J. Gravit. Physiol. 7 (2000) 13–14.

[7] J.E. Dunford, K. Thompson, F.P. Coxon, S.P. Luckman, F.M. Hahn, C.D. Poulter, F. H. Ebetino, M.J. Rogers, Structure-activity relationships for inhibition of farnesyl diphosphate synthase in vitro and inhibition of bone resorption in vivo by nitrogen-containing bisphosphonates, J. Pharmacol. Exp. Ther. 296 (2001) 235–242.

[8] J.M. Olmos, M.T. Zarrabeitia, J.L. Hernández, C. Sañudo, J. González-Macías, J. A. Riancho, Common allelic variants of the farnesyl diphosphate synthase gene influence the response of osteoporotic women to bisphosphonates, Pharmacogenomics J. 12 (3) (2012) 227–232, https://doi.org/10.1038/tpj.2010.88.

[9] P.H.L. de Freitas, T. Hasegawa, S. Takeda, M. Sasaki, C. Tabata, K. Oda, M. Li, H. Saito, N. Amizuka, Eldecalcitol, a second-generation vitamin D analog, drives bone minimodeling and reduces osteoclastic number in trabecular bone of ovariectomized rats, Bone 49 (3) (2011) 335–342, https://doi.org/10.1016/j.bone.2011.05.022.

[10] B. Ettinger, D.M. Black, B.H. Mitlak, R.K. Knickerbocker, T. Nickelsen, H.K. Genant, C. Christiansen, P.D. Delmas, J.R. Zanchetta, J. Stakkestad, C.C. Glüer, K. Krueger, F.J. Cohen, S. Eckert, K.E. Ensrud, L.V. Avioli, P. Lips, S.R. Cummings, Reduction of vertebral fracture risk in postmenopausal women with osteoporosis treated with raloxifene: Results from a 3-year randomized clinical trial, JAMA 282 (1999) 637–645, https://doi.org/10.1001/jama.282.7.637.

[11] J. Tuukkanen, A. Koivukangas, T. Jämsä, K. Sundquist, C.A. MacKay, S.C. Marks, Mineral density and bone strength are dissociated in long bones of rat osteopetrotic mutations, J. Bone Miner. Res. 15 (10) (2000) 1905–1911, https://doi.org/10.1359/jbmr.2000.15.10.1905.

[12] L.J. Melton, S. Khosla, E.J. Atkinson, W.M. O'Fallon, B.L. Riggs, Relationship of bone turnover to bone density and fractures, J. Bone Miner. Res. 12 (7) (1997) 1083–1091, https://doi.org/10.1359/jbmr.1997.12.7.1083.

[13] NIH Consensus Development Panel on Osteoporosis Prevention, Diagnosis, and Therapy, Osteoporosis prevention, diagnosis, and therapy, JAMA 285 (2001) 785-795, Doi: 10.1001/jama.285.6.785.

[14] J.J. Stepan, D.B. Burr, I. Pavo, A. Sipos, D. Michalska, J. Li, A. Fahrleitner-Pammer, H. Petto, M. Westmore, D. Michalsky, M. Sato, H. Dobnig, Low bone mineral density is associated with bone microdamage accumulation in postmenopausal women with osteoporosis, Bone 41 (3) (2007) 378–385, https://doi.org/10.1016/j.bone.2007.04.198.

[15] T.C. Kreipke, J.G. Garrison, J. Easley, A.S. Turner, G.L. Niebur, The roles of architecture and estrogen depletion in microdamage risk in trabecular bone, J. Biomech. 49 (14) (2016) 3223–3229, https://doi.org/10.1016/j.jbiomech.2016.08.009.

[16] G. Boivin, Y. Bala, A. Doublier, D. Farlay, L.G. Ste-Marie, P.J. Meunier, P.D. Delmas, The role of mineralization and organic matrix in the microhardness of bone tissue from controls and osteoporotic patients, Bone 43 (3) (2008) 532–538, https://doi.org/10.1016/j.bone.2008.05.024.

[17] D. Faibish, S.M. Ott, A.L. Boskey, Mineral changes in osteoporosis: A review, Clin. Orthop. Relat. Res. 443 (2006) 28–38, https://doi.org/10.1097/01.blo.0000200241.14684.4e.

[18] N. Mathavan, M.J. Turunen, M. Tägil, H. Isaksson, Characterising bone material composition and structure in the ovariectomized (OVX) rat model of osteoporosis, Calcif. Tissue Int. 97 (2) (2015) 134–144, https://doi.org/10.1007/s00223-015-9991-7.

[19] M. Saito, K. Marumo, Collagen cross-links as a determinant of bone quality: A possible explanation for bone fragility in aging, osteoporosis, and diabetes mellitus, Osteoporosis Int. 21 (2) (2010) 195–214, https://doi.org/10.1007/s00198-009-1066-z.

[20] A. Shiraishi, S. Miyabe, T. Nakano, Y. Umakoshi, M. Ito, M. Mihara, The combination therapy with alfacalcidol and risedronate improves the mechanical property in lumbar spine by affecting the material properties in an ovariectomized rat model of osteoporosis, BMC Musculoskelet Disord 10 (1) (2009), https://doi.org/10.1186/1471-2474-10-66.

[21] R. Ozasa, T. Ishimoto, S. Miyabe, J. Hashimoto, M. Hirao, H. Yoshikawa, T. Nakano, Osteoporosis changes collagen/apatite orientation and Young's modulus in vertebral cortical bone of rat, Calcif. Tissue Int. 104 (4) (2019) 449–460, https://doi.org/10.1007/s00223-018-0508-z.

[22] T. Nakano, K. Kaibara, Y. Tabata, N. Nagata, S. Enomoto, E. Marukawa, Y. Umakoshi, Unique alignment and texture of biological apatite crystallites in typical calcified tissues analyzed by microbeam x-ray diffractometer system, Bone 31 (4) (2002) 479–487, https://doi.org/10.1016/S8756-3282(02)00850-5.

[23] T. Ishimoto, T. Nakano, Y. Umakoshi, M. Yamamoto, Y. Tabata, Degree of biological apatite *c*-axis orientation rather than bone mineral density controls mechanical function in bone regenerated using recombinant bone morphogenetic protein-2, J. Bone Miner. Res. 28 (5) (2013) 1170–1179, https://doi.org/10.1002/jbmr.1825.

[24] Y. Shinno, T. Ishimoto, M. Saito, R. Uemura, M. Arino, K. Marumo, T. Nakano, M. Hayashi, Comprehensive analyses of how tubule occlusion and advanced glycation end-products diminish strength of aged dentin, Sci. Rep. 6 (2016) srep19849, https://doi.org/10.1038/srep19849.

[25] R. Ozasa, A. Matsugaki, T. Ishimoto, S. Kamura, H. Yoshida, M. Magi, Y. Matsumoto, K. Sakuraba, K. Fujimura, H. Miyahara, T. Nakano, Bone fragility via degradation of bone quality featured by collagen/apatite micro-arrangement in human rheumatic arthritis, Bone 155 (2022) 116261, https://doi.org/10.1016/j.bone.2021.116261.

[26] T. Moriishi, R. Ozasa, T. Ishimoto, T. Nakano, T. Hasegawa, T. Miyazaki, W. Liu, R. Fukuyama, Y. Wang, H. Komori, X. Qin, N. Amizuka, T. Komori, Osteocalcin is necessary for the alignment of apatite crystallites, but not glucose metabolism, testosterone synthesis, or muscle mass, PLoS Getet. 16 (2020), e1008586, https://doi.org/10.1371/journal.pgen.1008586.

[27] T. Wakamatsu, Y. Iwasaki, S. Yamamoto, K. Matsuo, S. Goto, I. Narita, J.J. Kazama, K. Tanaka, A. Ito, R. Ozasa, T. Nakano, C. Miyakoshi, Y. Onishi, S. Fukuma, S. Fukuhara, H. Yamato, M. Fukagawa, T. Akizawa, Type-I Angiotensin II Receptor Blockade Reduces Uremia-induced Deterioration of Bone Material Properties, J. Bone Miner. Res. 36 (2021) 67–79, https://doi.org/10.1002/jbmr.4159.

[28] Y. Tanaka, A. Kubota, M. Matsusaki, T. Duncan, Y. Hatakeyama, K. Fukuyama, A. J. Quantock, M. Yamato, M. Akashi, K. Nishida, Anisotropic mechanical properties of collagen hydrogels induced by uniaxial-flow for ocular applications, J. Biomater. Sci. Polym. Ed. 22 (11) (2011) 1427–1442, https://doi.org/10.1163/092050610X510542.

[29] B. Viswanath, R. Raghavan, U. Ramamurty, N. Ravishankar, Mechanical properties and anisotropy in hydroxyapatite single crystals, Scr. Mater. 57 (4) (2007) 361–364, https://doi.org/10.1016/j.scriptamat.2007.04.027.

[30] D. Adams, S.A. Swanson, Direct measurement of local pressures in the cadaveric human hip joint during simulated level walking, Ann. Rheum. Dis. 44 (10) (1985) 658–666, https://doi.org/10.1136/ard.44.10.658.

[31] R. Ozasa, M. Nakatsu, A. Moriguchi, K. Sasaki, T. Ishimoto, M. Okada, T. Matsumoto, T. Nakano, Analysis of bone regeneration based on the relationship between the orientations of collagen and apatite in mouse femur, Mater. Trans. 61 (2) (2020) 381–386, https://doi.org/10.2320/matertrans.MT-M2019341.

[32] W.J. Landis, K.J. Hodgens, J. Arena, M.J. Song, B.F. McEwen, Structural relations between collagen and mineral in bone as determined by high voltage electron microscopic tomography, Microsc. Res. Tech. 33 (1996) 192–202, https://doi.org/10.1002/(SICI)1097-0029(19960201)33:2<192::AID-JEMT9>3.0.CO;2-V.

[33] J.S. Nyman, S. Uppuganti, A.J. Makowski, B.J. Rowland, A.R. Merkel, J.A. Sterling, T.L. Bredbenner, D.S. Perrien, Predicting mouse vertebra strength with micro-computed tomography-derived finite element analysis, Bonekey Rep. 4 (2015) 664, https://doi.org/10.1038/bonekey.2015.31.

[34] H. Iida, S. Fukuda, Age-related changes in bone mineral density, cross-sectional area and strength at different skeletal sites in male rats, J. Vet. Med. Sci. 64 (1) (2002) 29–34, https://doi.org/10.1292/jvms.64.29.

[35] T. Ohata, H. Maruno, S. Ichimura, Changes over time in callus formation caused by intermittently administering PTH in rabbit distraction osteogenesis models, J. Orthop. Surg. Res. 10 (1) (2015), https://doi.org/10.1186/s13018-015-0228-2.

[36] R. Ozasa, A. Matsugaki, Y. Isobe, T. Saku, H.-S. Yun, T. Nakano, Construction of human induced pluripotent stem cell-derived oriented bone matrix microstructure by using in vitro engineered anisotropic culture model, J. Biomed. Mater. Res. A 106 (2) (2018) 360–369, https://doi.org/10.1002/jbm.a.36238.

[37] Y.-X. Wang, J.F. Griffith, H. Zhou, K.C. Choi, V.W.Y. Hung, D.K.W. Yeung, L. Qin, A.T. Ahuja, Rat lumbar vertebrae bone densitometry using multidetector CT, Eur. Radiol. 19 (4) (2009) 882–890, https://doi.org/10.1007/s00330-008-1219-z.

[38] T. Ishimoto, B. Sato, J.-W. Lee, T. Nakano, Co-deteriorations of anisotropic extracellular matrix arrangement and intrinsic mechanical property in c-src deficient osteopetrotic mouse femur, Bone 103 (2017) 216–223, https://doi.org/10.1016/j.bone.2017.06.023.

[39] A. Sekita, A. Matsugaki, T. Ishimoto, T. Nakano, Synchronous disruption of anisotropic arrangement of the osteocyte network and collagen/apatite in melanoma bone metastasis, J. Struct. Biol. 197 (3) (2017) 260–270.

[40] J.Y. Rho, G.M. Pharr, Effects of drying on the mechanical properties of bovine femur measured by nanoindentation, J. Mater. Sci. Mater Med. 10 (1999) 485–488, https://doi.org/10.1023/A:1008901109705.

[41] A.J. Bushby, V.L. Ferguson, A. Boyde, Nanoindentation of bone: comparison of specimens tested in liquid and embedded in polymethylmethacrylate, J. Mater. Res. 19 (1) (2004) 249–259, https://doi.org/10.1557/jmr.2004.19.1.249.

[42] T. Ishimoto, T. Nakano, Y. Yamamoto, Y. Tabata, Biomechanical evaluation of regenerating long bone by nanoindentation, J. Mater. Sci. Mater. Med. 22 (4) (2011) 969–976, https://doi.org/10.1007/s10856-011-4266-y.

[43] W.C. Oliver, G.M. Pharr, An improved technique for determining hardness and elastic modulus using load and displacement sensing indentation experiments, J. Mater. Res. 7 (6) (1992) 1564–1583.

[44] A.R. Villanueva, Stain technology a bone stain for osteoid seams in fresh, unembedded, mineralized bone, Biotech. Histochem. 49 (1) (1974) 1–8, https://doi.org/10.3109/10520297409116928.

[45] V. Bentolila, T.M. Boyce, D.P. Fyhrie, R. Drumb, T.M. Skerry, M.B. Schaffler, Intracortical remodeling in adult rat long bones after fatigue loading, Bone 23 (3) (1998) 275–281, https://doi.org/10.1016/S8756-3282(98)00104-5.

[46] R.M. O'brien, A caution regarding rules of thumb for variance inflation factors, Qual. Quan. 41 (2007) 673–690, https://doi.org/10.1007/s11135-006-9018-6.

[47] D.E. Hughes, K.R. Wright, H.L. Uy, A. Sasaki, T. Yoneda, D.G. Roodman, G.R. Mundy, B.F. Boyce, Bisphosphonates promote apoptosis in murine osteoclasts in vitro and in vivo, J. Bone Miner. Res. 10 (10) (1995) 1478–1487, https://doi.org/10.1002/jbmr.5650101008.

[48] C. Vitté, H. Fleisch, H.L. Guenther, Bisphosphonates induce osteoblasts to secrete an inhibitor of osteoclast-mediated resorption, Endocrinology 137 (6) (1996) 2324–2333, https://doi.org/10.1210/endo.137.6.8641182.

[49] F. Bauss, R.C. Schimmer, Ibandronate: The first once-monthly oral bisphosphonate for treatment of postmenopausal osteoporosis, Ther. Clin. Risk. Manag. 2 (2006) 3–18.

[50] S. Sakai, H. Takaishi, K. Matsuzaki, H. Kaneko, M. Furukawa, Y. Miyauchi, A. Shiraishi, K. Saito, A. Tanaka, T. Taniguchi, T. Suda, T. Miyamoto, Y. Toyama, 1-Alpha, 25-dihydroxy vitamin D3 inhibits osteoclastogenesis through IFN-beta-dependent NFATc1 suppression, J. Bone Miner. Metab. 27 (6) (2009) 643–652, https://doi.org/10.1007/s00774-009-0084-4.

[51] H. Takasu, A. Sugita, Y. Uchiyama, N. Katagiri, M. Okazaki, E. Ogata, K. Ikeda, c-Fos protein as a target of anti-osteoclastogenic action of vitamin D, and synthesis of new analogs, J. Clin. Invest. 116 (2006) 528–535, https://doi.org/10.1172/JCI24742.

[52] J. Kikuta, S. Kawamura, F. Okiji, M. Shirazaki, S. Sakai, H. Saito, M. Ishii, Sphingosine-1-phosphate-mediated osteoclast precursor monocyte migration is a critical point of control in antibone-resorptive action of active vitamin D, Proc. Natl. Acad. Sci. U. S. A. 110 (17) (2013) 7009–7013, https://doi.org/10.1073/pnas.1218799110.

[53] S. Harada, T. Mizoguchi, Y. Kobayashi, Y. Nakamichi, S. Takeda, S. Sakai, F. Takahashi, H. Saito, H. Yasuda, N. Udagawa, T. Suda, N. Takahashi, Daily administration of eldecalcitol (ED-71), an active vitamin D analog, increases bone mineral density by suppressing RANKL expression in mouse trabecular bone, J. Bone Miner. Res. 27 (2) (2012) 461–473, https://doi.org/10.1002/jbmr.555.

[54] T.H. Smit, The use of a quadruped as an in vivo model for the study of the spine - Biomechanical considerations, Eur. Spine J. 11 (2) (2002) 137–144, https://doi.org/10.1007/s005860100346.

[55] J. Homminga, B. Van-Rietbergen, E.M. Lochmüller, H. Weinans, F. Eckstein, R. Huiskes, The osteoporotic vertebral structure is well adapted to the loads of daily life, but not to infrequent "error" loads, Bone 34 (3) (2004) 510–516, https://doi.org/10.1016/j.bone.2003.12.001.

[56] Z. Zhang, Y. Chen, L. Xiang, Z. Wang, G.G. Xiao, D. Ju, Diosgenin protects against alveolar bone loss in ovariectomized rats via regulating long non-coding RNAs,

Experimental and Therapeutic Medicine 16 (2018) 3939–3950, https://doi.org/10.3892/etm.2018.6681.

[57] P.L. Salmon, C. Ohlsson, S.J. Shefelbine, M. Doube, Structure model index does not measure rods and plates in trabecular bone, Front. Endocrinol. (Lausanne) 6 (2015) 162, https://doi.org/10.3389/fendo.2015.00162.

[58] T. Ishimoto, K. Kawahara, A. Matsugaki, H. Kamioka, T. Nakano, Quantitative evaluation of osteocyte morphology and bone anisotropic extracellular matrix in rat femur, Calcif. Tissue Int. 109 (4) (2021) 434–444, https://doi.org/10.1007/s00223-021-00852-1.

[59] M. Tanaka, A. Matsugaki, T. Ishimoto, T. Nakano, Evaluation of crystallographic orientation of biological apatite in vertebral cortical bone in ovariectomized cynomolgus monkeys treated with minodronic acid and alendronate, J. Bone Miner. Metab. 34 (2) (2016) 234–241, https://doi.org/10.1007/s00774-015-0658-2.

[60] S. Miyabe, T. Ishimoto, T. Nakano, Preferential orientation of biological apatite in normal and osteoporotic human vertebral trabeculae, J. Phys. Conf. Ser. 165 (2009) 012087, https://doi.org/10.1088/1742-6596/165/1/012087.

[61] K. Tai, M. Dao, S. Suresh, A. Palazoglu, C. Ortiz, Nanoscale heterogeneity promotes energy dissipation in bone, Nat. Mater. 6 (6) (2007) 454–462, https://doi.org/10.1038/nmat1911.

[62] E. Schacht, L. Dukas, F. Richy, Combined therapies in osteoporosis: bisphosphonates and Vitamin D-hormone analogs, J. Musculoskelet. Neuronal Interact. 7 (2007) 174–184.

[63] S. Ochiai, Y. Nishida, Y. Higuchi, D. Morita, K. Makida, T. Seki, K. Ikuta, S. Imagama, Short-range UV-LED irradiation in postmenopausal osteoporosis using ovariectomized mice, Sci. Rep. 11 (2021) 7875, https://doi.org/10.1038/s41598-021-86730-0.

[64] T.S. Kaastad, O. Reikerås, V. Halvorsen, J.A. Falch, K.J. Obrant, L. Nordsletten, Vitamin D deficiency and ovariectomy reduced the strength of the femoral neck in rats, Calcif. Tissue Int. 69 (2) (2001) 102–108, https://doi.org/10.1007/s00223-001-0009-2.